JOURNAL OF GEOPHYSICAL RESEARCH, VOL. 100, NO. A4, PAGES 5835–5852, APRIL 1, 1995

Linear and nonlinear properties of ULF waves driven by ring-beam distribution functions

K. Killen, N. Omidi,[1] D. Krauss-Varban, and H. Karimabadi

Department of Electrical and Computer Engineering, University of California, San Diego, La Jolla

Abstract. The problem of the excitation of obliquely propagating magnetosonic waves which can steepen up (also known as shocklets) is considered. Shocklets have been observed upstream of the Earth's bow shock and at comets Giacobini-Zinner and Grigg-Skjellerup. Linear theory as well as two-dimensional (2-D) hybrid (fluid electrons, particle ions) simulations are used to determine the properties of waves generated by ring-beam velocity distributions in great detail. The effects of both proton and oxygen ring-beams are considered. The study of instabilities excited by a proton ring-beam is relevant to the region upstream of the Earth's bow shock, whereas the oxygen ring-beam corresponds to cometary ions picked up by the solar wind. Linear theory has shown that for a ring-beam, four instabilities are found, one on the nonresonant mode, one on the Alfvén mode, and two along the magnetosonic/whistler branch. The relative growth rate of these instabilities is a sensitive function of parameters. Although one of the magnetosonic instabilities has maximum growth along the magnetic field, the other has maximum growth in oblique directions. We have studied the competition of these instabilities in the nonlinear regime using 2-D simulations. As in the linear limit, the nonlinear results are a function of beam density and distribution function. By performing the simulations as both initial value and driven systems, we have found that the outcome of the simulations can vary, suggesting that the latter type of simulations is needed to address the observations. A general conclusion of the simulation results is that field-aligned beams do not result in the formation of shocklets, whereas ring-beam distributions can.

1. Introduction

The existence of suprathermal ions that flow back upstream along the interplanetary magnetic field from the Earth's bow shock has been well established [e.g., *Asbridge et al.*, 1968; *Lin et al.*, 1974]. These ions fall into several distinct classes. The earliest classification distinguished only between "reflected" and "diffuse" populations [*Gosling et al.*, 1978; *Bonifazi and Moreno*, 1981]. Reflected ions are well-collimated, field-aligned beams with sharply peaked energy spectra. Diffuse ions, on the other hand, are more isotropic with broad angular distributions in velocity space and flatter energy spectra. The field-aligned beams exist in a narrow region near the ion foreshock, where the angle between the magnetic field and the shock normal, θ_{Bn}, is approximately 50°; the diffuse ions are found in a broad region extending deep into the foreshock, where θ_{Bn} is much smaller [*Greenstadt et al.*, 1980; *Paschmann et al.*, 1981]. Later, a third category of ions was identified and labeled as "intermediate" due to the fact that their energy spectra and angular distributions have characteristics that fall between those of the reflected and diffuse ions [*Paschmann et al.*, 1979]. Still more recently, another class of ions, termed the "gyrating ions," has been identified [*Gurgiolo et al.*, 1981; *Eastman et al.*, 1981]. These ions are distinguished from other classes by their bulk gyromotion around the magnetic field, meaning that the peak in their distribution lies at a nonzero pitch angle relative to the magnetic field. Gyrating ion distributions range from being gyrophase bunched, meaning that they have a very narrow range of gyrophases, to nearly gyrotropic. In a comparison between intermediate and gyrating ions, *Fuselier et al.* [1986] noted that the two populations are similar in shock geometry and spatial location and that methods used in earlier studies (e.g., moments and energy time spectrograms) cannot distinguish between the two populations. Consequently, nearly half of the events originally classified as intermediate ion events are actually gyrating ion events.

Spacecraft observations have also shown the presence of low-frequency magnetic fluctuations upstream of the Earth's bow shock [*Greenstadt et al.*, 1968; *Fairfield*,

[1] Also at California Space Institute, University of California, San Diego, La Jolla.

Paper number 94JA02899.
0148-0227/95/94JA-02899$05.00

1969; *Hoppe et al.*, 1981; *Hoppe and Russell*, 1983]. At smaller amplitudes, the waves are sinusoidal and transverse. At larger amplitudes, the waves are strongly compressional and have a steepened form. The steepened waves, along with an associated high-frequency wave packet, have been termed "shocklets" by *Hoppe et al.* [1981]. These waves propagate toward the sun at small oblique angles ($\sim 30°$) relative to the interplanetary magnetic field (IMF) and are convected back by the solar wind [*Hoppe et al.*, 1981; *Hoppe and Russell*, 1983]. *Hoppe and Russel* [1983] have shown that the low-frequency waves propagate predominantly along the magnetosonic mode, while *Russell et al.* [1971] have shown that the higher-frequency discrete wave packets are on the whistler mode. Studies have shown that the smaller amplitude, sinusoidal waves are associated with the intermediate and gyrating ion populations, whereas shocklets are associated with the diffuse ion population [*Paschmann et al.*, 1979; *Hoppe et al.*, 1981; *Fuselier et al.*, 1986]. No association between low-frequency waves and the field-aligned ion beams has been found.

In the past decade a number of studies have been conducted to determine the mechanism responsible for the growth of the low-frequency waves and the formation of the intermediate and diffuse ion populations. It has been suggested that the source of intermediate and diffuse ions are the field-aligned beams, which undergo scattering as a result of wave-particle interactions [*Paschmann et al.*, 1979; *Bame et al.*, 1980; *Gary et al.*, 1981]. In this model, reflected ions excite magnetosonic waves via a resonant beam instability [*Gary et al.*, 1981]. When the ions are a beam, the waves are too small to be detected. As the waves grow, they scatter the beam particles. By the time the waves have amplified enough to be observed, the beam has scattered in energy and pitch angle such that the ions appear as an intermediate distribution and then finally as a diffuse distribution. This model is supported by the results of a hybrid (particle ions, fluid electrons) simulation performed by *Winske and Leroy* [1984], who showed that the evolution of an ion beam due to the resonant ion beam instability does produce distributions similar to those seen upstream of the bow shock. However, the more recent viewpoint is that the diffuse ions are generated directly at the quasi-parallel shock and may evolve from gyrating ion distributions [e.g., *Fuselier*, 1994].

Two main mechanisms have been proposed to account for the formation of gyrating ion distributions: specular reflection off the shock and particle trapping. In the former, a portion of incoming solar wind ions are specularly reflected off the bow shock, yielding a gyrophase-bunched ion beam [*Gosling et al.*, 1982; *Sckopke et al.*, 1983]. In a quasi-perpendicular geometry these ions are transmitted back into the shock, whereas in a quasi-parallel geometry the gyrating ions can travel further upstream of the shock. Within a few Earth radii, gyrophase mixing occurs due to a finite thermal spread, resulting in a more gyrotropic distribution. These ion distributions resemble a ring-beam in velocity space and are expected to be unstable to the generation of electromagnetic waves [*Thomsen et al.*, 1985]. Therefore, near the shock, gyrating ions should be gyrophase-bunched, and further out they should be more gyrotropic. Observational evidence of gyrating ion distributions is consistent with this model [*Gosling et al.*, 1982; *Thomsen et al.*, 1983b]. There exists, however, a population of gyrophase-bunched ions several Earth radii upstream of the shock, suggesting a mechanism other than shock reflection for their formation [*Gurgiolo et al.*, 1981]. To explain the presence of these ions, *Hoshino and Terasawa* [1985] suggested that the excitation of electromagnetic waves by the field-aligned beam can result in the trapping and gyrophase bunching of the beam. By comparing the phase relationship between the monochromatic ULF waves and the gyrophase bunched ions, *Fuselier et al.* [1986] were able to confirm this hypothesis.

Large amplitude, low-frequency magnetic fluctuations similar to those found in the Earth's foreshock region have also been observed at comet Giacobini-Zinner (GZ) by the ICE spacecraft [*Smith et al.*, 1986; *Tsurutani and Smith*, 1986a, b; *Gosling et al.*, 1986] and at comet Grigg-Skjellerup (GS) [*Glassmeier and Neubauer*, 1993]. In the case of the comet, the waves are excited by the interaction between the solar wind and the newly created cometary ions whose distribution is generally in the form of a ring-beam. Because of the more massive nature of the cometary ions (water group ions as opposed to protons), the waves have a lower frequency, i.e., near the water group cyclotron frequency [*Tsurutani and Smith*, 1986a, b].

Past linear theory studies based on ring-beam distributions such as those found at GZ and in the Earth's foreshock have shown the presence of a variety of instabilities. The type of instabilities found is a function of α, the angle between the solar wind flow and the ambient magnetic field. When $\alpha \sim 0°$, the distribution resembles a cold beam, and the dominant instabilities are the resonant and nonresonant ion/ion beam instabilities [e.g., *Gary et al.*, 1984; *Gary and Madland*, 1988]. When $\alpha \sim 90°$, the distribution is a cold ring, and left-hand ion cyclotron instabilities are found [e.g., *Gary and Madland*, 1988]. Between these two limits, the distribution is a ring-beam. This case is far more complex because there are two distinct sources of free energy. Because of this, depending on the parameters, a range of beam and ring instabilities can be found, but the right-hand instabilities tend to dominate [see *Winske et al.*, 1985; *Gary and Madland*, 1988; *Goldstein et al.*, 1990; *Wong et al.*, 1991].

Although observations and theoretical work have considerably improved our knowledge of wave-particle interactions in the foreshock and at comets, there are still a number of important issues which have not been resolved. For example, the proposed instability responsible for the initial disruption of the field-aligned beams, termed the right-hand resonant ion/ion instability by *Gary et al.* [1981], excites waves in a range of propagation angles, but maximum growth occurs along the magnetic field. The observed shocklets, however, prop-

agate at an oblique (~30°) angle. The resolution of this discrepancy is important because the nonlinear evolution of obliquely propagating magnetosonic waves can include the formation of shocklets, whereas the nonlinear evolution of parallel propagating magnetosonic waves does not [*Omidi and Winske*, 1990; *Akimoto et al.*, 1991]. To address this issue of oblique propagation, a number of models have been proposed. One such model introduced by *Hada et al.* [1987] and tested by *Le* [1991] is wave refraction. In this model, the parallel propagating waves generated by field-aligned beams are refracted to oblique propagation as they are convected into the region where diffuse ions are found. This is caused by the nonuniform index of refraction introduced by spatial variations in the plasma. This process is more likely to occur when there is a sharp boundary between the reflected ion region and the diffuse ion region and when there is a large angle between the ambient magnetic field and the solar wind flow. However, observations have shown that shocklets are a typical waveform and are also seen during periods when the IMF is nearly radial. *Le* [1991] has shown that in this geometry there is no sharp boundary between the field-aligned and diffuse ion populations, and therefore the refraction model does not seem to be supported. Other attempts at explaining the oblique nature of the waves involved searches for unstable modes with maximum growth at oblique angles. For example, *Brinca and Tsurutani* [1989] performed a linear theory analysis using a drifting bi-Maxwellian distribution function to model the cometary environment. They showed that islets of oblique growth unrelated to unstable parallel modes exist. However, the nature of this instability and the excited mode was not clear. In another study, *Goldstein et al.* [1990] were able to show that ring-beam distribution functions can result in unstable waves with maximum growth at oblique angles, but it is unclear if these waves are magnetosonic.

Motivated by these results, we have conducted a detailed analysis of instabilities associated with ring-beam distribution functions. As noted earlier, such a distribution function models both cometary ions as well as the gyrating ions at the foreshock. Preliminary results of this study were presented by *Omidi et al.* [1994], where it was shown that two low-frequency instabilities can excite magnetosonic waves, one with maximum growth at parallel propagation and the other with maximum growth in oblique directions. The parallel instability is a result of the beam part of the distribution and has properties similar to the right-hand resonant ion/ion instability. The oblique instability is mostly a result of the temperature anisotropy associated with the ring and grows as a result of cyclotron resonance at higher harmonics. On the basis of these findings and the results of two-dimensional (2-D) hybrid (fluid electrons, particle ions) simulations, we have proposed that the large amplitude, compressional waves found at planetary foreshocks and at comet GZ are generated by the interaction between gyrating ions and the solar wind. Although field-aligned beams can also excite magnetosonic waves, it is unlikely that compressional waves are generated by this population.

The purpose of this paper is to present the results of a continuation of the study by *Omidi et al.* [1994]. We have performed a detailed linear analysis of ULF waves excited by ring-beam distributions as well as 2-D hybrid simulations to investigate their nonlinear evolution. The linear theory study shows that a number of different modes are excited by ring-beam distributions, and the simulations are used to determine how these modes compete in the nonlinear regime. The results of the linear theory study are presented in section 2, and the results of the simulations are presented in section 3. Section 4 provides a summary of our findings.

2. Linear Theory

Ring-beam distributions exist at comets and upstream of the bow shock, as do magnetosonic waves which steepen to form shocklets [*Hoppe and Russell*, 1983; *Tsurutani et al.*, 1987]. In order to further our understanding of the connection between the two, we have conducted a detailed linear theory study of ring-beam distributions with parameters that fit the two environments. Past linear theory studies have shown that ring-beam distributions can give rise to a variety of instabilities, ranging from beam instabilities to ion cyclotron instabilities, depending on the angle between the IMF and the solar wind flow. We have used linearized Vlasov theory to examine what modes are excited by a ring-beam distribution and how their characteristics (e.g., growth rate, angle of maximum growth) are affected when beam parameters, such as density or velocity, are varied. The linear theory study presented in this paper is based on a distribution function of the form:

$$f_b(v_\parallel, v_\perp) \propto \exp\left(-(v_\parallel - v_{\parallel b})^2/{v_{th}}^2\right)\delta(v_\perp - v_{\perp b}). \quad (1)$$

Here $v_\parallel$ and $v_\perp$ are the velocities parallel and perpendicular to the magnetic field, respectively; v_{th} is the thermal velocity in the parallel direction, and $\vec{v}_b$ is the beam velocity, which has components parallel and perpendicular to the magnetic field. This distribution represents a ring-beam with a thermal spread in the parallel direction. Although a transverse thermal spread would be expected in a real situation, we do not expect the lack of thermal spread in this case to have a substantial effect on the results. In fact, we have looked at the properties of a drifting bi-Maxwellian with a temperature anisotropy such that $T_\perp > T_\parallel$ and found similar instabilities to those reported here.

A preliminary study based on this distribution in which the ion beam is composed of singly ionized oxygen O^+ ($m_b = 16m_p$), modeling a cometary environment, has been described by *Omidi et al.* [1994]. The parameters used here are the same as those used in the previous study. The beam velocity is $v_b = 4V_A$ (where V_A is the Alfvén speed) and $v_{th} = v_{\perp b}/7$. The beam makes an angle of 30° with the ambient magnetic field, the background (solar wind) electron and ion betas (ra-

tio of plasma to magnetic pressure) are both unity, and the beam density is $n_b = 0.05n_o$, where n_o is the background density. Here we summarize the results presented in that paper and provide further details.

Under the conditions mentioned above, two unstable solutions exist along the magnetosonic branch. The four panels of Figure 1 show the real (ω) and imaginary (γ) parts of the frequency as a function of wave number k for four different wave normal angles (Θ_{Bk}) from 2° to 40°. The frequencies are normalized to the proton gyrofrequency (Ω_p) and the wave number is normalized to the proton inertial length (c/ω_p). A comparison among the panels gives a clear picture of the linear properties of the magnetosonic mode for a ring-beam distribution. At parallel propagation, one instability can be seen, which is labeled beam-driven (BD) magnetosonic. This instability is similar to that of a pure beam and grows due to cyclotron resonance. At larger wave normal angles ($\Theta_{Bk} = 22°$), a second solution (shown by a thick dashed line), termed a beam mode (BM), also becomes unstable. Although the real parts of the dispersion curve cross for $\Theta_{Bk} = 22°$, the two modes stay decoupled with the magnetosonic mode having the larger growth rate at all k. Note, however, the double-hump nature of γ, which results due to the

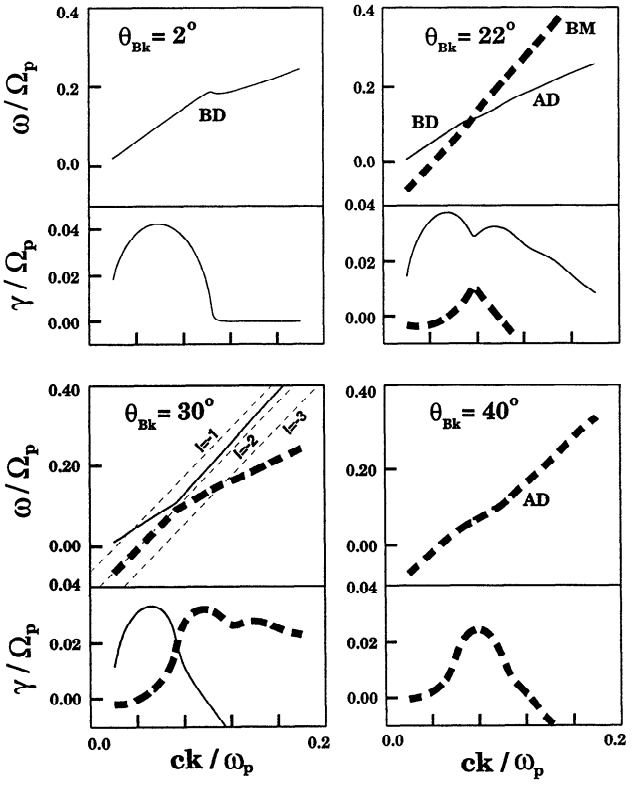

Figure 1. Plots of the real (ω) and imaginary (γ) parts of the frequency as a function of wave number (k) for four wave normal angles (Θ_{Bk}) and a 5% oxygen ring-beam. BD and AD correspond to the beam-driven (BD) and anisotropy-driven (AD) magnetosonic modes, respectively, and BM corresponds to the beam resonance mode. Three different cyclotron resonance conditions are plotted for $\Theta_{Bk} = 30°$.

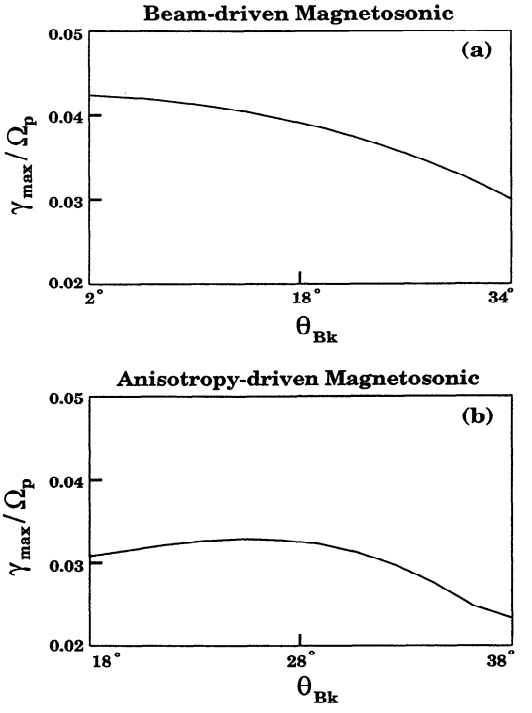

Figure 2. Plots of the maximum growth rate (γ_{max}) as a function of wave normal angle (Θ_{Bk}) for (a) the beam-driven part of the magnetosonic mode and (b) the anisotropy-driven magnetosonic mode.

crossing of the two modes. The two humps correspond to what are two separate instabilities at slightly larger wave normal angles. The wave number at which these two solutions cross corresponds to the dip between the two humps, as well as the growth peak along the beam mode ($k \sim 0.075$). By $\Theta_{Bk} = 30°$, the magnetosonic branch has coupled with this beam mode and two distinct instabilities with comparable growth rates can be seen. The first is the beam-driven resonant instability, which is also seen at parallel propagation. The second has been called the anisotropy-driven instability (AD) because it is driven primarily by the ring, or anisotropy, part of the distribution, although the beam component is still necessary in order for the resonance condition to be satisfied [*Omidi et al.*, 1994]. Note that the maximum growth of both instabilities occurs on the magnetosonic branch at k values below and above the crossing point of the two branches. The three dotted lines in this panel (labeled $l = -1$, -2, and -3) correspond to the cyclotron resonance conditions for the first, second, and third harmonics, where

$$\omega = k_{\|} v_{b\|} + l\Omega_b. \quad (2)$$

The second harmonic beam mode has coupled with the magnetosonic whistler branch. Note also that there are two humps in the growth rate of the anisotropy-driven instability (dotted line), which indicates that even higher harmonics should be important. By $\Theta_{Bk} = 40°$ the beam-driven mode has stablized, but the anisotropy-driven mode still has a sizable growth rate. Details of this transition are a function of beam parameters. Figure 2 compares the growth rates of the two instabilities

maximized over k as a function of wave normal angle. The top panel shows that the beam-driven instability has a larger maximum growth rate which occurs at parallel propagation, while the anisotropy-driven instability has a slightly smaller growth rate which peaks at more oblique angles (around $\Theta_{Bk} = 26°$ in this case). The fact that the beam-driven magnetosonic mode has maximum growth at parallel propagation is indicative of the fact that this instability is essentially the same as the right-hand resonant ion/ion instability. The anisotropy-driven mode has maximum growth at oblique angles because it grows due to resonance at second and higher harmonics.

We have also found that in addition to magnetosonic waves, this type of distribution can excite other types of waves, depending on the beam parameters. For example, we have confirmed that, as stated by *Winske et al.* [1985], ring-beam distributions can excite waves along the nonresonant mode if the beam density is high enough. Similarly, the Alfvén ion-cyclotron mode can also become unstable. For the parameters shown here, both of these instabilities have larger maximum growth rates than the magnetosonic instabilities. The top two panels in Figure 3 show the real (ω) and the imaginary

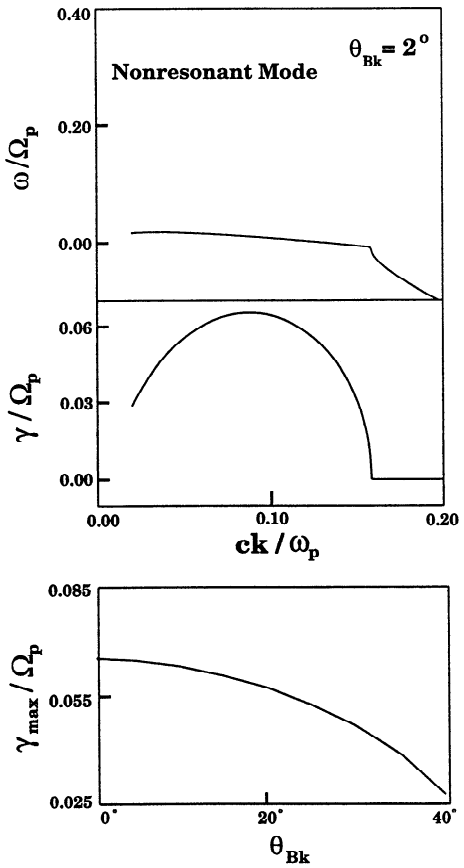

Figure 3. Plots of the real (ω) and imaginary (γ) parts of the frequency as a function of wave number (k) at one wave normal angle ($\Theta_{Bk} = 2°$) for the nonresonant mode for a 5% oxygen ring-beam. Also, the maximum growth rate (γ_{max}) of the nonresonant mode as a function of wave normal angle.

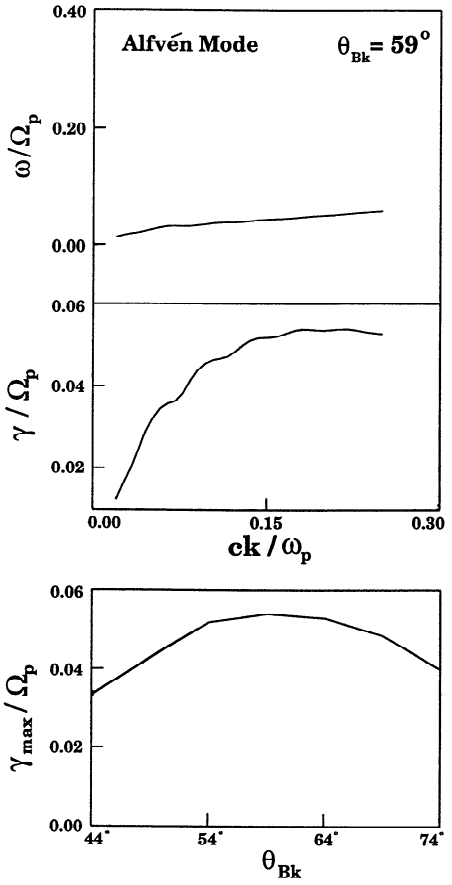

Figure 4. Plots of the real (ω) and imaginary (γ) parts of the frequency as a function of wave number (k) for one wave normal angle ($\Theta_{Bk} = 59°$) for the Alfvén mode of a 5% oxygen ring-beam. Also, maximum growth rate (γ_{max}) of the Alfvén mode as a function of wave normal angle.

(γ) parts of the frequency as a function of wave number k for parallel propagation ($\Theta_{Bk} = 2°$) along the nonresonant mode. The bottom panel shows the maximum growth rate (γ_{max}) as a function of propagation angle. This instability excites waves at much lower frequencies than the magnetosonic instabilities and also has a higher maximum growth rate, around 0.065 Ω_p, which drops off quickly as the wave normal angle is increased. However, our study has shown that as the beam density is decreased, the maximum growth rate of the nonresonant instability decreases to the point that it is insignificant compared to the magnetosonic.

It has been shown that pure ring distributions can excite Alfvén waves via the Alfvén ion-cyclotron anisotropy instability [*Gary and Madland*, 1988]. We have found that a ring-beam distribution is also capable of exciting Alfvén waves. Figure 4 shows panels similar to Figure 3 for the Alfvén mode. This instability also excites waves at somewhat lower frequencies than the magnetosonic mode, and it has a sizable growth rate, around 0.055 Ω_p, at slightly larger wave numbers. An examination of the maximum growth rate as a function of wave normal angle (bottom panel) indicates that Alfvén waves

can be excited over a large range of oblique propagation directions. With these parameters, the maximum growth occurs at $\Theta_{Bk} \sim 60°$. At such large angles this is the only existing instability we have found. On the basis of the linear properties outlined above, we expect the nonresonant mode to be dominant at lower wave normal angles and the Alfvén mode to be dominant at higher wave normal angles. The magnetosonic instabilities have lower growth rates for the full range of angles. However, as the parameters vary, so do the growth rates and thus so do the instabilities we would expect to dominate. This fact will be of importance when we describe the results of our simulations.

In order to properly model the reflected gyrating ion beams at the Earth's bow shock, we have studied a second case in which the ion beam is composed of protons H^+ ($m_b = m_p$). We have chosen the beam density to be $n_b = 0.01 n_o$, where n_o is the background density, based on observational data [*Bonifazi and Moreno*, 1981]. The beam velocity is taken to be $v_b = 12 V_A$ in the rest frame of the solar wind. All temperatures are comparable, and both the electron and ion beta are $\beta_e = \beta_i = 0.5$. The beam makes an angle of 30° with the background magnetic field. We have found that three separate instabilities are excited under these parameters. Two of the instabilities are along the magnetosonic mode, and one is along the nonresonant mode. The forward propagating Alfvén mode is damped in this case.

Figure 5 shows four panels similar to Figure 1; the instabilities shown in these dispersion relations are on the magnetosonic mode. The four panels show the real (ω) and imaginary (γ) parts of the frequency as a function of wave number k for four different wave normal angles (Θ_{Bk}) from 2° to 42°. The two instabilities are very similar to the instabilities on the magnetosonic branch in the oxygen case described above. At parallel propagation, there is a single instability, once again called the beam-driven instability, but as the wave normal angle is increased, a second, anisotropy-driven instability which has maximum growth at oblique angles, appears. Although the two instabilities are along two separate branches, maximum growth rates of both instabilities occur on the magnetosonic mode. Despite the similarities, there are also differences between this case and the oxygen case. First, the coupling between the magnetosonic branch and the beam mode occurs at lower wave normal angles. At $\Theta_{Bk} = 22°$, the two modes have already coupled, and both the beam-driven instability and the anisotropy-driven instability have well-defined growth peaks which do not overlap in k. A slight second hump in the growth rate of the anisotropy-driven instability is apparent. By $\Theta_{Bk} = 32°$, the second hump is much more pronounced, and unlike the oxygen case, the anisotropy-driven instability still exhibits a smaller growth than the beam-driven. In this panel are also shown the cyclotron resonance conditions for the first, second, and third harmonics (dotted lines labeled $l = -1$, -2, and -3). The coupling of the magnetosonic mode with the second and the third harmonic beam modes is apparent. By $\Theta_{Bk} = 42°$, the beam-driven instability still persists, and the anisotropy-driven instability has become larger. However, there is no angle at which the anisotropy-driven instability has a larger growth than the beam-driven instability. This point is illustrated in Figure 6, which shows the maximum growth rate of both instabilities as a function of wave normal angle. The beam driven instability has a relatively flat maximum growth over a large range of angles, with the maximum $\gamma \sim 0.2\,\Omega_p$ at 0°. The anisotropy-driven instability has maximum growth at approximately 42°, where $\gamma \sim 0.13\,\Omega_p$.

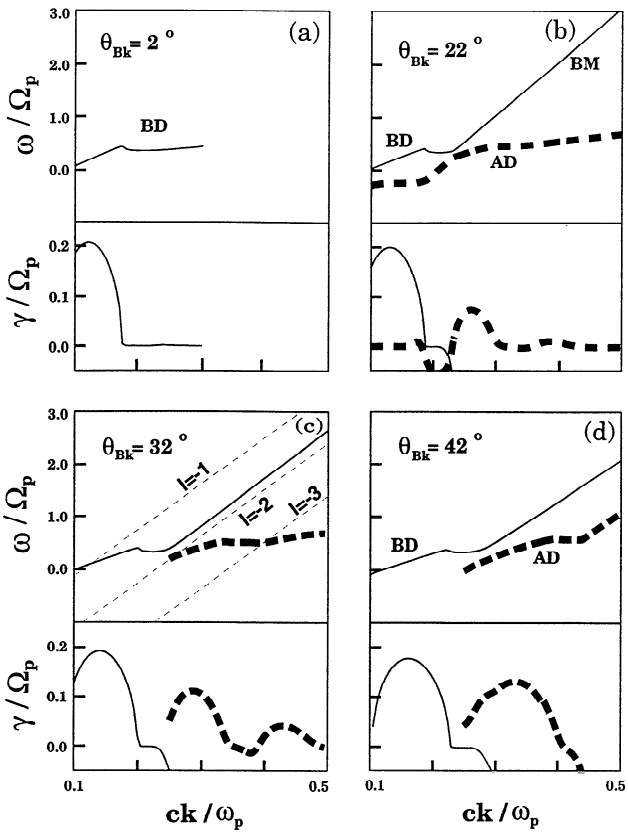

Figure 5. Plots of the real (ω) and imaginary (γ) as a function of wave number (k) for four wave normal angles (Θ_{Bk}) and a 1% proton ring-beam. BD and AD correspond to the beam-driven and anisotropy-driven magnetosonic modes, respectively; BM corresponds to the beam resonance mode. Three beam cyclotron resonance conditions are plotted for $\Theta_{Bk} = 30°$.

Another notable difference between the previously studied oxygen case and the proton case is that in the former the nonresonant mode has the largest maximum growth rate, whereas in the latter it has an insignificant growth rate. Figure 7, like Figures 3 and 4, shows the real (ω) and imaginary (γ) parts of the frequency as a function of wave number k for parallel propagation ($\Theta_{Bk} = 2°$), along the nonresonant mode, as well as its maximum growth rate as a function of wave normal angle. The growth rate is nonnegative for a very short range of wave numbers. The maximum growth rate as a function of wave normal angle (bottom panel), which

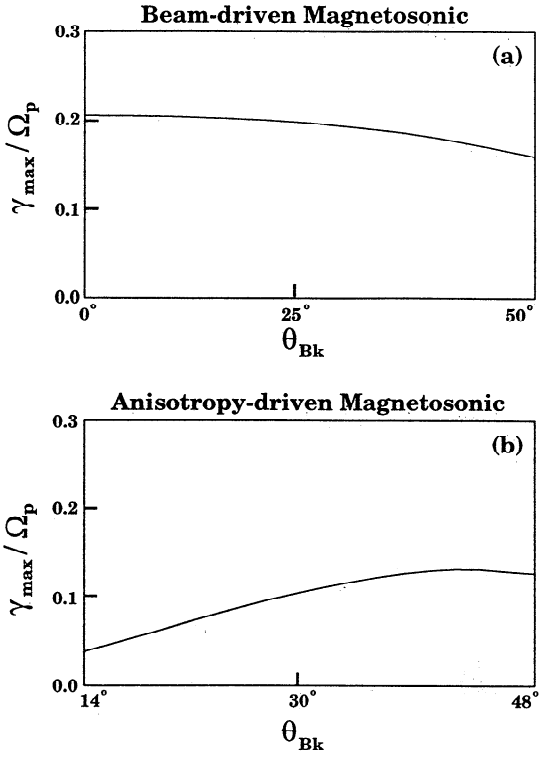

Figure 6. Maximum growth rate (γ_{max}) of (a) the beam-driven and (b) the anisotropy-driven magnetosonic mode as a function of wave normal angle (Θ_{Bk}).

occurs at parallel propagation, is more than a factor of 10 smaller than those of the magnetosonic instabilities. Therefore the magnetosonic instabilities should dominate the wave spectrum in these regimes.

3. Two-Dimensional Simulations

3.1. Oxygen Beam Case

Having examined the linear properties of waves driven by ring-beam distributions, we now turn to the issue of the nonlinear evolution of these waves. To understand how the four instabilities outlined above compete in the nonlinear regime, we have performed two sets of 2-D hybrid simulations. In the first set of simulations, the ion beam species is singly ionized oxygen. The results of these simulations were first presented in *Omidi et al.* [1994], and here we provide a more detailed analysis. The second set of simulations have a proton beam interacting with a proton background as would be seen upstream of the bow shock. All of the simulations are either initial value or driven. In an initial value simulation, the beam ions are present at $t = 0$, and in a driven simulation, the beam ions are injected uniformly in space and time such that the full beam density is achieved at the end of the simulation. Two types of initial value simulations have been performed, one type corresponding to a cool field-aligned beam, the other corresponding to a ring-beam distribution. The simulation parameters are similar to those used in the linear theory study presented above. We first consider the oxygen simulations.

Linear theory of a cool field-aligned beam indicates that maximum growth of both the resonant and nonresonant instabilities occurs parallel to the magnetic field. Thus one would expect that in a 2-D simulation employing a cool field-aligned beam, parallel waves would dominate, and no steepening would be observed. To test this expectation, we have performed a simulation in which the beam ions are a cool field-aligned beam of oxygen ions. The system is doubly periodic in the $X-Y$ plane with a size of 400×85 c/ω_p and a cell size of 1 c/ω_p in each direction. The background ions are represented by 20 particles per cell. The beam has a density of $n_b = 0.05n_o$, where n_o is the background density. The background magnetic field is at 30° with respect to the X axis, while the oxygen beam is injected with velocity of $v_b = 4V_A$ along the magnetic field, giving an overall beam distribution. Although the waves do indeed

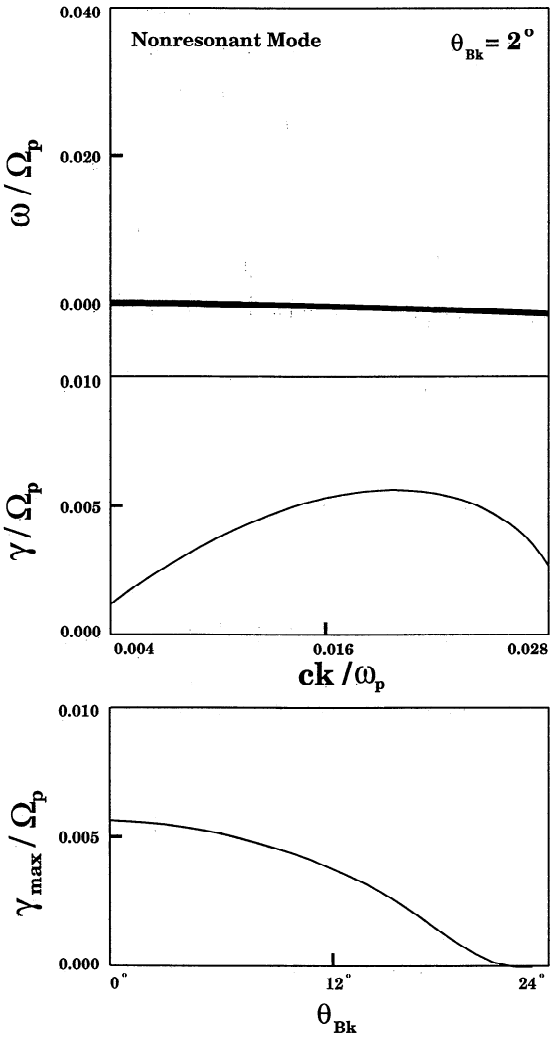

Figure 7. Plot of the real (ω) and imaginary (γ) parts of the frequency as a function of wave number (k) for a wave normal angle of $\Theta_{Bk} = 2°$ of the nonresonant mode for a 1% proton ring-beam. Also shown are the maximum growth rate (γ_{max}) as a function of wave normal angle.

reach a large amplitude ($\delta B/B_o \sim 1$), no steepening is observed. Figure 8 shows B_y as a function of X and Y at two times. The top panel corresponds to a time just before the saturation of the instability, and the bottom panel corresponds to a time just after the saturation point. In both panels, the waves are large amplitude and sinusoidal, indicating that there is no steepening involved in the evolution of these waves. This lack of steepening is explained by an examination of power as a function of propagation angle, in which it is shown that first parallel and then later oblique waves are excited (Figure 9). The two panels of Figure 9 show power as a function of propagation angle for 2 times in the simulation. In the first panel it can be seen that early in the simulation ($\Omega_p t \sim 75$) parallel waves are excited. The second panel shows that later in the simulation ($\Omega_p t \sim 120$) the power has shifted into more oblique directions. Note that since the magnetic field makes an angle of 30° with the X axis, power at $\Theta_{kx} = 30°$ corresponds to the direction parallel to the magnetic field ($\Theta_{Bk} = 0°$), while power at $\Theta_{kx} = 0°$ corresponds to waves propagating at 30° with respect to the magnetic field. Although parallel waves are initially dominant, later in the simulation oblique waves are also excited. Since parallel waves are noncompressional, they are not expected to form shocklets. In order to determine which instabilities are responsible for the growth of the waves, we have performed a Fourier analysis in space and time which provides us with a power spectrum in $\omega-k$ space. The results of this analysis (not shown here) are that at early times ($70 \leq \Omega_p t \leq 110$) only the nonresonant mode is present in the system. Later in the simulations ($110 \leq \Omega_p t \leq 150$) some parallel propagating resonant mode is also present, but the nonresonant mode remains dominant. No shocklets are seen because no oblique magnetosonic waves are generated in this simulation.

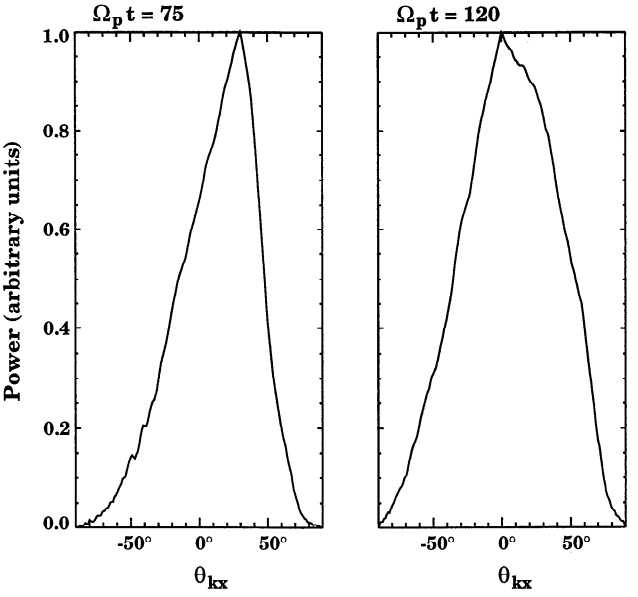

Figure 9. Power as a function of angle for an initial value field-aligned oxygen beam simulation. The power starts out parallel to the magnetic field and later moves to oblique angles.

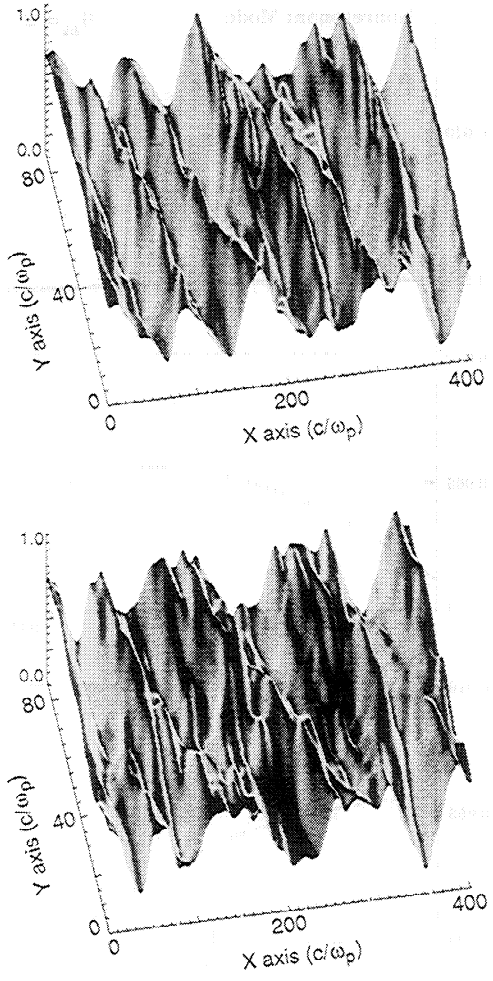

Figure 8. Surface plots of a transverse component of the magnetic field B_y as a function of X and Y for an initial value field-aligned oxygen beam. The top panel corresponds to a time of peak growth while the bottom panel corresponds to a somewhat later time. Despite their large amplitude, at both times the waves have a sinusoidal form and have not steepened.

We now turn to the results of a simulation is which the ions have a ring-beam velocity distribution. The parameters used in this simulation are similar to those used in Figures 1–4. The top panel in Figure 10 shows the time evolution of the magnetic field energy for the entire run. There are two separate growth phases, one which saturates at $\Omega_p t \sim 135$ and a second one which saturates at $\Omega_p t \sim 185$. Examining power as a function of propagation angle at these two times (bottom two panels) shows that at the first saturation point the power peaks at $\Theta_{kx} \sim 30°$ and at the second saturation point, the power peaks at $\Theta_{kx} = 0°$. Keeping in mind that the for the entire run. There are two separate growth phases, one which saturates at $\Omega_p t \sim 135$, and a second one which saturates at $\Omega_p t \sim 185$. Examining power as a function of propagation angle at these two times (bottom two panels) shows that at the first saturation point the power peaks at $\Theta_{kx} \sim 30°$

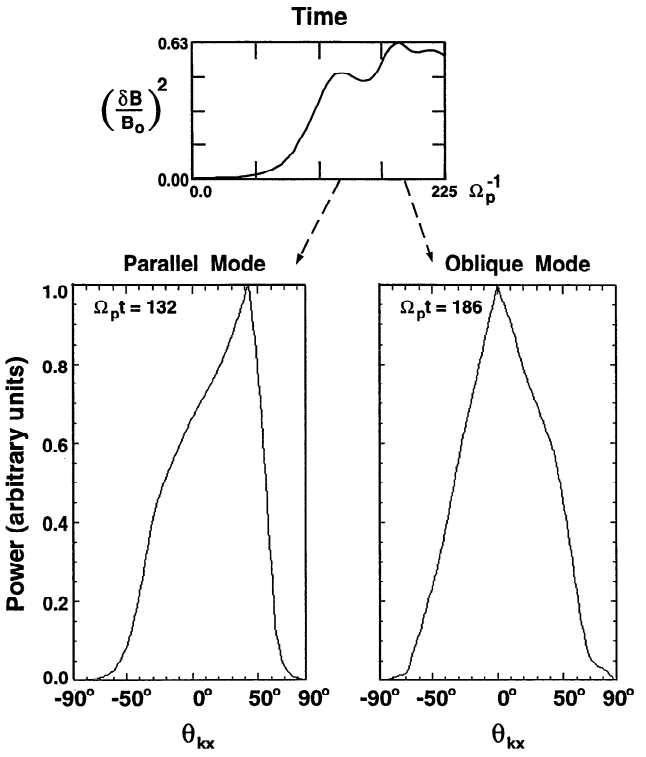

Figure 10. The top panel shows the time history of the fluctuating magnetic field energy for an initial value 5% oxygen ring-beam. Two peaks can be seen at times $\Omega_p t \sim 132$ and 186. Plots of power as a function of Θ_{kx} at these two times (bottom panels) show the initial dominance of parallel propagating wave (nonresonant mode) followed by the dominance of oblique waves (beam-driven and anisotropy-driven magnetosonic mode). Note that the ambient magnetic field makes an angle of 30° with the X axis.

and at the second saturation point the power peaks at $\Theta_{kx} = 0°$. Keeping in mind that the magnetic field is at 30° with respect to the X axis, this evidence indicates that first parallel and then later obliquely growing waves dominate the spectrum. In order to determine which specific instabilities are responsible for the two growth phases, we have performed a Fourier transform in space and time to obtain the power spectrum. Figure 11 shows the power spectra for nearly parallel propagating waves at two time intervals. The left panel shows the power spectrum for the full duration of the run ($0 \leq \Omega_p t \leq 225$), while the right panel corresponds to times after the first saturation ($135 \leq \Omega_p t \leq 225$). The solid lines are the dispersion curves obtained from linear theory for these parameters. It can be seen that in the left panel most of the power resides on the nonresonant mode, with some residual power on the beam-driven magnetosonic. This matches our expectations from the linear theory study, which shows two instabilities having maximum growth along the magnetic field, and the nonresonant one having the larger magnitude. The right panel, which shows the power spectrum for the latter part of the run, demonstrates that most of the power resides in the beam-driven instability, and almost none resides in the nonresonant. The contrast between these two panels clearly shows that the nonresonant mode is excited first and is dominant only in the first part of the run. During the second growth phase, the beam-driven magnetosonic waves are excited. Figure 12 shows two similar panels for oblique propagating waves. The left panel shows the power spectrum for the entire run ($0 \leq \Omega_p t \leq 225$). There is significant power in the nonresonant mode, as well as both the beam-driven and anisotropy-driven magnetosonic modes. The right panel shows the power spectrum for the time interval starting at the first saturation point and extending to the end of the run ($135 \leq \Omega_p t \leq 225$). There is no longer any power in the nonresonant mode, and the magnetosonic waves are dominant. This is again an indication that the nonresonant mode grows in the first growth phase, whereas the magnetosonic modes grow in the latter part of the simulation. Although in the second growth phase there is power in both of the magnetosonic instabilities, the beam-driven dominates the anisotropy-driven. The power of the beam-driven instability in the parallel and oblique directions is comparable, although it is slightly larger in the oblique direction. The dominance of oblique waves is easily explained because there are two instabilities contributing to them, whereas in the parallel case there is only one (the beam-driven). It should be noted that at no point is the Alfvén mode dominant in this simulation, despite the fact that its growth rate is larger than the magnetosonic mode. This is most likely due to ion scattering by the nonresonant mode, which is initially dominant, and by the time it saturates the distribution has changed enough that the Alfvén mode can no longer be driven unstable. This explanation is consistent with the evolution of the beam distribution function in time. Figure 13 shows the $(v_\parallel, v_\perp)$ phase space distribution of the ring-beam ions early in the run and at the two saturation points. In Figure 13a, which corresponds to an early time in the run when the waves are of low amplitude, the average parallel velocity is comparable to the original distribution, and some pitch angle scattering has occurred. Figure 13b corresponds to the first saturation point. By this time there has been enough pitch angle scattering and energy diffusion to form a half shell, causing the saturation of the nonresonant instability. However, there is still a sizable amount of free energy left in the system to excite magnetosonic waves. Figure 13c corresponds to the second saturation point where the distribution has scattered into a full shell and is no longer unstable. It is customary to assume that pickup ions scatter in pitch angle on a constant energy shell before scattering in energy. However, Figure 13 indicates that scattering in pitch angle and in energy occur simultaneously. These results are consistent with observations at comet Halley [e.g., *Karimabadi et al.*, 1994].

The results presented here suggest the following mechanism for the evolution of the system. Initially, (for sufficient beam density) the nonresonant instability is dominant and parallel waves are excited. As these

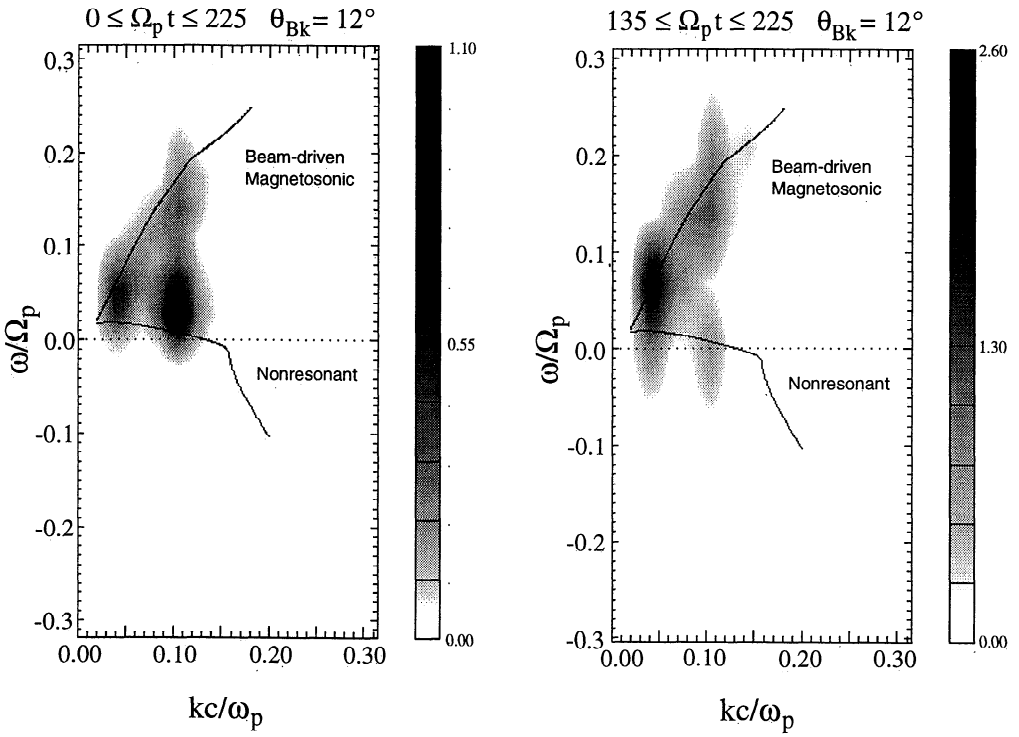

Figure 11. Power spectrum of B_y for parallel propagating waves ($\Theta_{Bk} = 12°$) for two time intervals with the dispersion relations for the magnetosonic and the nonresonant modes. Note that the fast Fourier transform (FFT) performed here averages over wave amplitude. The fact that peak power in the right panel is greater than peak power in the left panel indicates that the wave amplitude from $135 \leq \Omega_p t \leq 225$ is greater than that from $0 \leq \Omega_p t \leq 135$. Therefore the FFT performed in the left panel, which averages over the entire time of the simulation, results in a lower peak power.

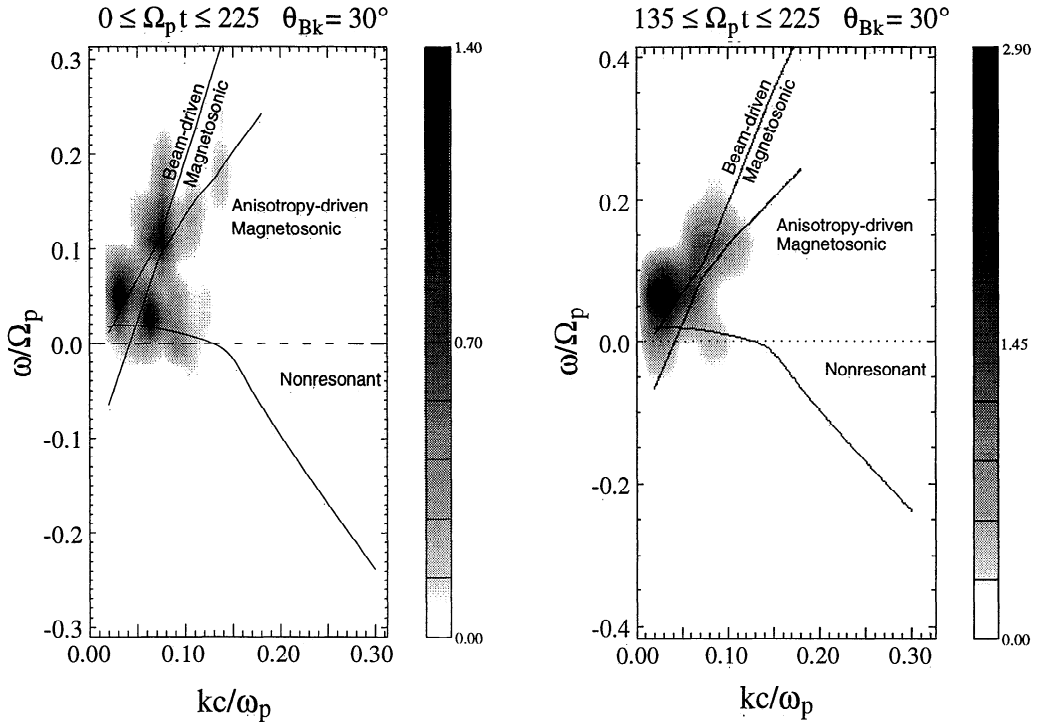

Figure 12. Power spectrum for oblique propagating waves (wave normal angle $\Theta_{Bk} = 30°$) for two time intervals. Also shown are the dispersion relations for the magnetosonic and the nonresonant modes for 5% oxygen.

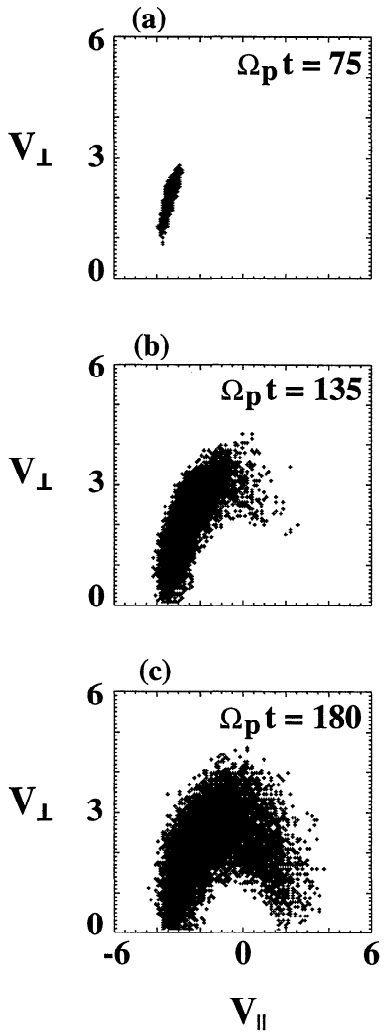

Figure 13. Phase space density plots of 5% oxygen at three times. (b) At time $\Omega_p t \sim 135$ the ions have undergone sufficient pitch-angle scattering for the nonresonant mode to have saturated. But the magnetosonic mode is still unstable and becomes saturated at (c) $\Omega_p t \sim 180$.

waves grow, particles undergo pitch angle scattering and energy diffusion until the nonresonant mode stablizes; at this point the particles are in a half-shell distribution, and there is still enough free energy in the system for magnetosonic waves to grow via the two instabilities. During this second growth phase, the power moves into oblique directions and oblique magnetosonic waves grow until the second saturation point is reached. It should be noted that in this case, no steepening of waves is observed. The lack of steepening may be related to the fact that the obliquely growing waves do not dominate until late in the run, and thus they do not have enough time or power to steepen before the distribution has scattered into a shell and lost its free energy.

The lack of steepening in the initial value simulation does not introduce a contradiction between theory and observation because the initial value system is not directly applicable to physical settings such as comets and planetary foreshocks. A more realistic situation for comets is one in which the beam ions are created uniformly in space and time (radial variation of the ion production rate can be ignored for local simulations). For this reason we have performed a driven oxygen ring-beam simulation in which the final beam density is $n_b = 0.05 n_o$. In a driven system, particles are continually injected such that the full beam density is achieved at the end of the run. Therefore the average beam density is smaller than for the initial value simulation. All of the parameters are the same as in the initial value simulation with the exception that the beam ions are injected along the X axis, meaning that they have velocities of $4\times$ cos 30 V_A parallel to and $4\times$ sin 30 V_A perpendicular to the magnetic field. It has been shown by *Omidi et al.* [1994] that from early on the dominant waves in the system propagate at an angle of $\Theta_{Bk} \sim 30^o$ with respect to the magnetic field. Plate 1 shows a transverse component of the magnetic field (B_y) as a function of X and Y at $\Omega_p t \sim 200$. The five white lines are cuts through X at five different values of Y. Three shocklets are apparent. They all have a distinct steepened edge as well as a reasonably large coherence length in Y (i.e. of the order of the wavelength). Thus in this more realistic simulation, steepening of the magnetosonic waves is observed. In order to determine the instability responsible for generating the waves, we have performed a power spectrum analysis, the results of which are shown in Figure 14. The panel on the left shows the power spectrum for waves propagating at 30° and the dispersion relations for the nonresonant as well as the beam-driven and the anisotropy-driven magnetosonic modes for a 5% oxygen beam. It is evident that the excited waves are magnetosonic with maximum power on the beam-driven part of the mode. However, since in this simulation the beam density varies with time, there is still the question of how the varying beam density affects the mode identification. The rightmost panel zooms in on the power and shows the dispersion relations for three beam densities which are valid at different times in the run. All three match the power spectrum. Therefore we conclude that the steepened waves generated in this simulation are on the magnetosonic mode. The lack of parallel propagating nonresonant waves that dominated the initial value simulation discussed earlier can be explained by the fact that here the average beam density is considerably lower. According to *Winske and Gary* [1986] and our own studies, the maximum growth rate of the nonresonant instability decreases considerably as the beam density is decreased. Thus by the time the beam density is large enough for the nonresonant instability to have a significant growth rate, the particles have already scattered enough to stablize that mode. For this reason, only magnetosonic waves are generated. Another interesting result of this simulation is the dominance of the oblique magnetosonic waves. As was noted in the initial value simulation, the magnetosonic waves were observed to grow in both parallel and oblique directions with the latter waves having more power. In the driven simulations, the power in the oblique waves is

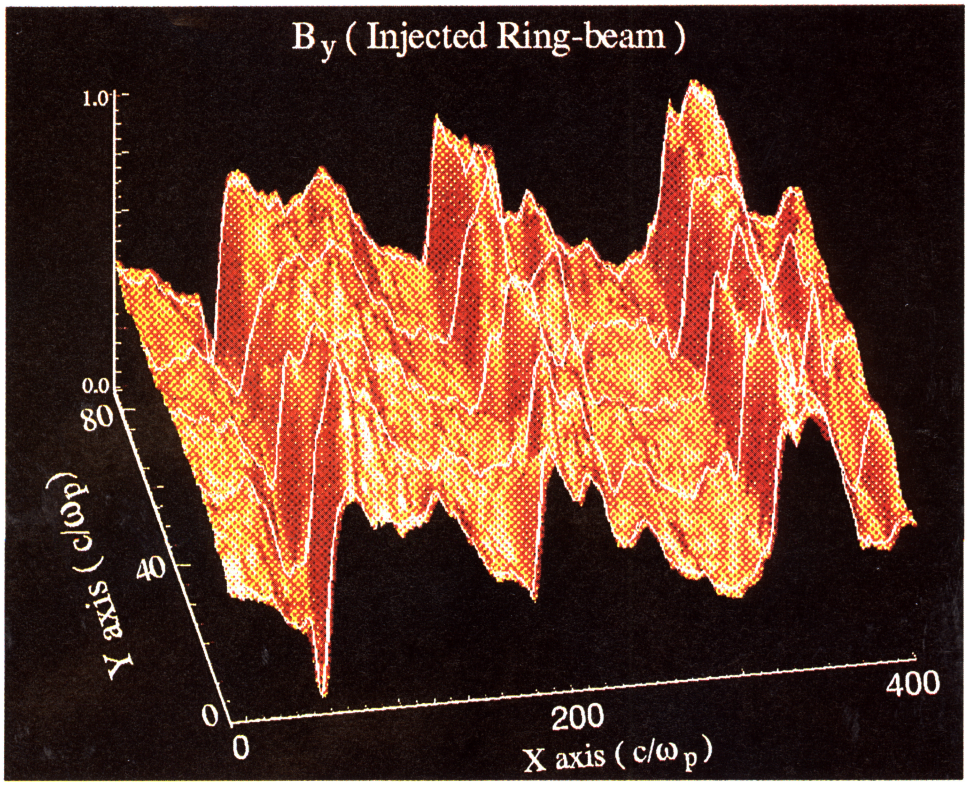

Plate 1. Surface plot of a transverse component of the magnetic field B_y as a function of X and Y for a driven ring-beam distribution. The waves have steepened to form three shocklets.

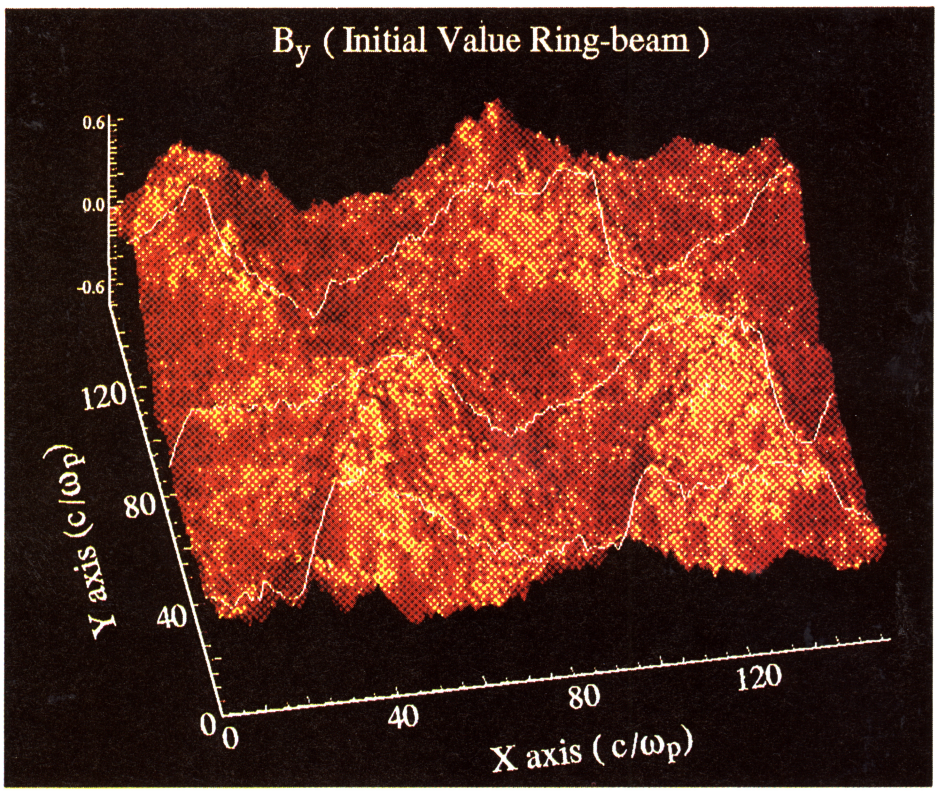

Plate 2. Surface plot of a driven 1% proton ring-beam at time $\Omega_p t = 60$ normalized to the background magnetic field. Three white slices show some steepening of the waves in space.

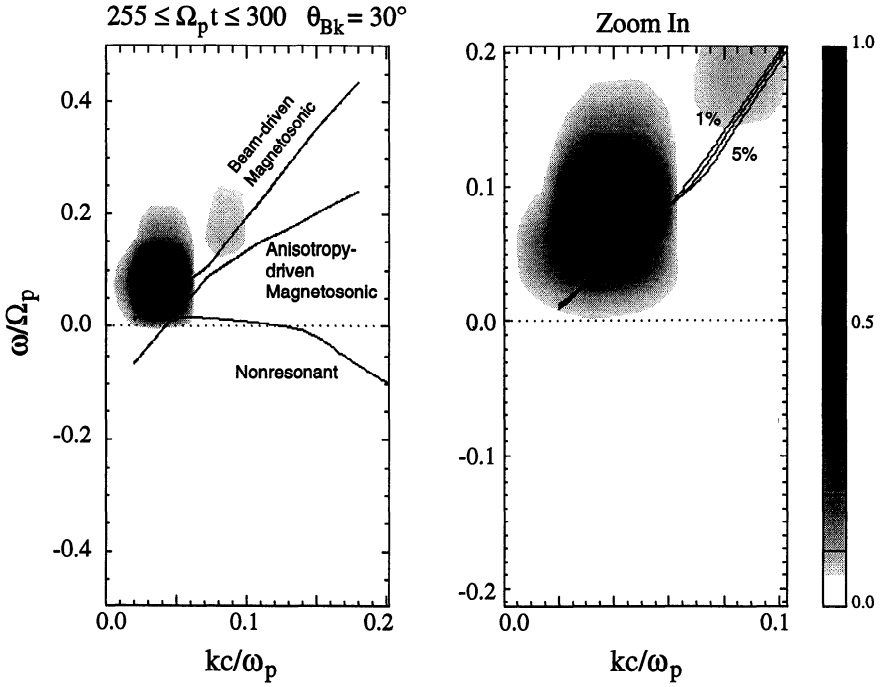

Figure 14. Power spectrum for a driven 5% oxygen simulation. The first panel shows the power and mode lines for $\Theta_{Bk} = 30°$. The second panel shows the power and the beam-driven (BD) magnetosonic dispersion solution for three different beam densities.

considerably larger. Although the exact reason for this behavior is not known, a number of possibilities can be mentioned. One is that the driven simulations correspond to having a source term in the Vlasov equation. This may modify the growth rates of the magnetosonic instabilities such that the parallel waves do not grow as much. The other possibility is that the continuous scattering of the injected ions leads to a distribution function which deviates to a considerable degree from a ring-beam distribution function. This again could modify the linear theory results so that parallel waves do not grow as much as in the initial value simulation. Finally, the distribution function of the injected ions is not gyrotropic, which again could modify the results of linear theory.

The driven oxygen simulation is a good local model for the cometary setting in that the beam ions are injected uniformly in space; given the similarity between the driven simulation and the actual ion production occurring at comets, it seems reasonable to assume that the mechanisms studied here are valid there as well. This may then explain the generation of shocklets at comet GZ. However, foreshock settings are somewhat different and require separate modeling. In the next subsection the results of simulations with proton beams are presented.

3.2. Proton Beam Case

Two types of simulations were done with a proton beam, one using a field-aligned beam velocity distribution, and the other using a ring-beam distribution. Both are initial value simulations in which the beam density starts out at 1% of the background density, and no additional beam particles are injected. In order to properly model a driven system for the foreshock, a nonperiodic system is needed. Results of this type of calculations will be presented in the future. Despite the lack of driven simulations for the foreshock, initial value simulations can still provide further insights about the generation of shocklets in that environment.

As with the oxygen beam, we first consider a simulation employing a field-aligned proton beam. The system is doubly periodic in X and Y with size $700 \times 700 c/\omega_p$ in the $-Y$ plane. The background plasma is represented by 25 particles per cell, where the cell size is 1 c/ω_p, and the beam is 1% of the background density. Both the magnetic field and v_b are along the X axis, where $v_b = 12V_A$ in the rest from of the background plasma, i.e., the solar wind. Preliminary analysis has shown that with these parameters waves are excited through a wide range of propagation angles, from 0° to ~ 60°, but maximum power occurs at parallel propagation. As per our regular methodology, we have determined which mode is dominant by looking at power as a function of propagation angle as well as the power spectrum. Although there are two growth phases in the simulation, they cannot be distinguished by their power as a function of propagation angle. Throughout the run, power peaks at parallel propagation and decreases for increasingly large propagation angles, forming a broad cone. On the basis of the power spectrum, we have concluded that the resonant mode is dominant over the nonresonant mode for the full range of propagation angles. This can be explained by the fact that at such a low beam density, the growth rate for the nonresonant mode is much smaller than that of the resonant. The waves

themselves are sinusoidal in shape, lacking the steepened edge characteristic of shocklets. This is because the majority of the power in the system resides in the parallel propagating waves, which lack a compressional component and would therefore not be expected to form shocklets. The first panel of Figure 15 shows k_x versus k_y as well as two lines defining the propagation angles of 60° and −60°. It can be seen that the power exists throughout the broad region enclosed by the two lines, meaning that waves are propagating through the full range of angles. The second panel shows the maximum growth rate of the magnetosonic mode as a function of propagation angle. Notice that the curve is nearly flat up to 60°, which means that waves are likely to grow in a broad cone around the magnetic field. These results agree with simulation results, indicating that the full range of waves is excited via linear processes.

Having determined that a field-aligned beam cannot form shocklets, we now turn to the results of a simulation in which the injected protons have a ring-beam distribution. As we described earlier in this paper, in a linear analysis of the proton ring-beam distribution, only two instabilities are seen, the beam-driven and the anisotropy-driven. To examine how these two instabilities compete in the nonlinear regime when the nonresonant mode is not present, an initial value 2-D simulation was performed. The system is doubly periodic in X and Y with size $500 \times 500\ c/\omega_p$ in the $X - Y$ plane. The particles are initialized with a velocity at an angle of 30° with respect to the X axis (which is here parallel to the magnetic field), meaning that the beam ions have velocities of $12\times \cos 30 V_A$ parallel to and $12\times \sin 30 V_A$ perpendicular to the magnetic field, giving an overall ring-beam distribution. Aside from these two exceptions, all of the parameters are the same as those used for the field-aligned proton beam simulation.

From early on, there are two groups of waves present which propagate in different directions. The left panel of Figure 16 shows the intensity plot of B_z in which the interference pattern between the two sets of waves can be seen. The second panel shows a plot of power versus wave normal angle for time $\Omega_p t \sim 18$. There are two peaks at oblique angles, $\Theta_{Bk} = 18°$ and $\Theta_{Bk} = -42°$. However, we note that the angular resolution of this system is of the order of ±14°, so it is difficult to assign terms such as parallel or oblique to the 18° peak. The second peak, on the other hand, can definitely be classified as oblique. Fourier analysis demonstrates that at this time two instabilities are present. Figure 17 shows the results of this analysis. The first panel corresponds to the peak at $\Theta_{Bk} = 18°$. This power lies along the unstable part of the beam-driven magnetosonic mode, in agreement with our expectations based on linear theory. The second panel shows the power at 42°. The majority of the power is still along the beam-driven instability, but there is also power in the anisotropy-driven mode. More power lies in oblique direction because of the combined effects of both instabilities. Examination of one of the transverse components of the magnetic field (B_y) just before saturation ($\Omega_p t = 60$) shows that the wave

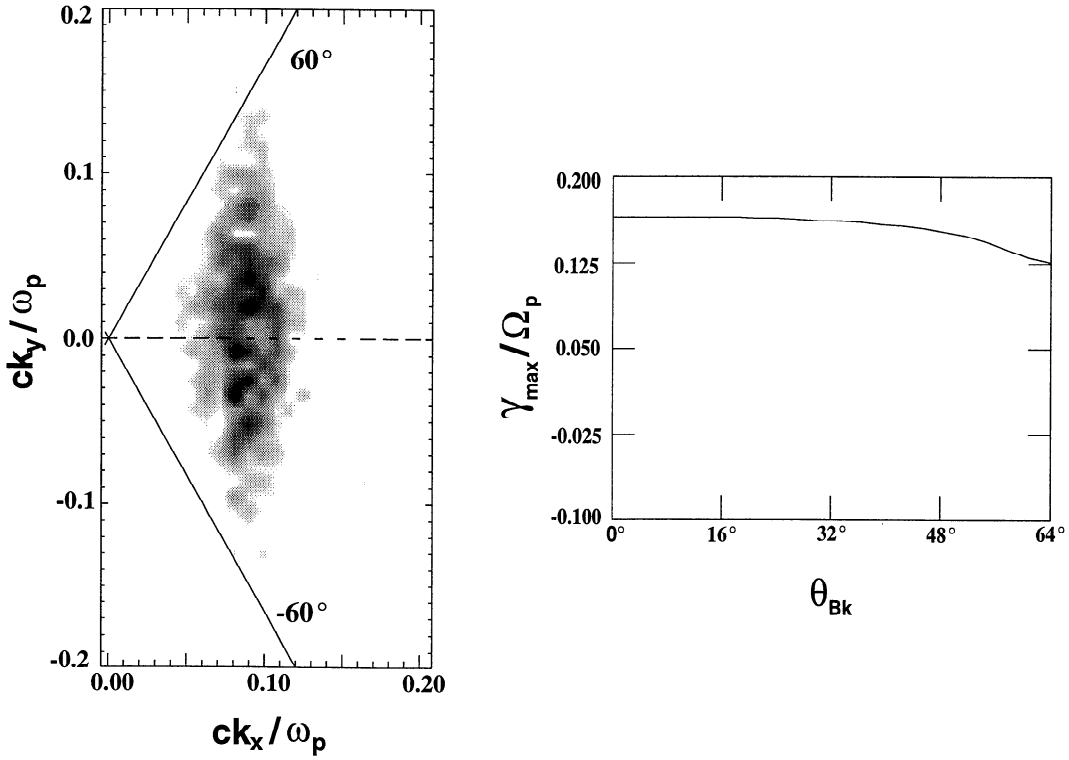

Figure 15. Wave propagation in an initial value field-aligned proton simulation. The first panel shows k_x versus k_y, The second panel shows the maximum growth rate ($\gamma_{\max}$) as a function of wave normal angle.

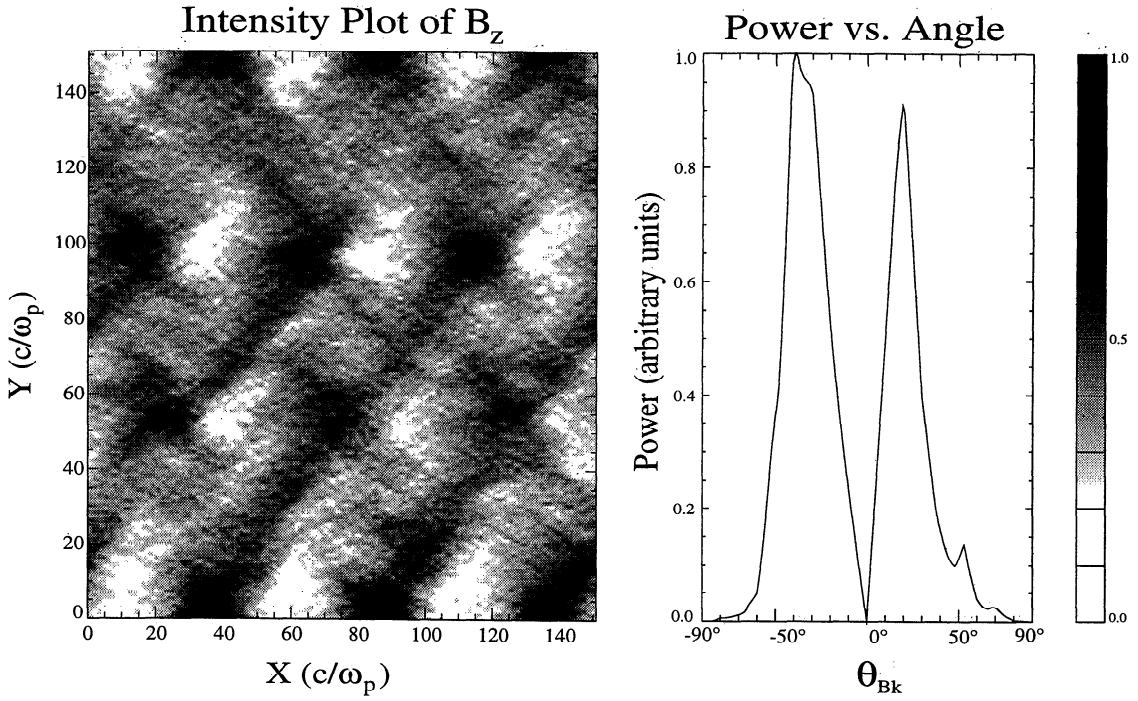

Figure 16. Intensity plot of B_z as a function of X and Y for an initial value 1% proton ring-beam. Also shown is power versus wave normal angle. Here the background magnetic field in the X direction.

fronts are curved rather than planar in nature. This is due to the interaction of the forward and backward propagating waves in Y (see Plate 2). Plate 2 shows the amplitude of B_y as a function of X and Y. The three white slices demonstrate that there is some steepening of the wavefronts, but their coherence in the transverse direction is not very long (about 20 c/ω_p). According to *Le* [1991], the coherence length of the shocklets in the direction perpendicular to the solar wind velocity is of the order of an Earth radii, which is comparable to a wavelength. Here the ratio of the coherence length to the wavelength of the waves is about 0.5, which is somewhat smaller than that found by *Le* [1991]. One reason for this may be the presence of parallel prop-

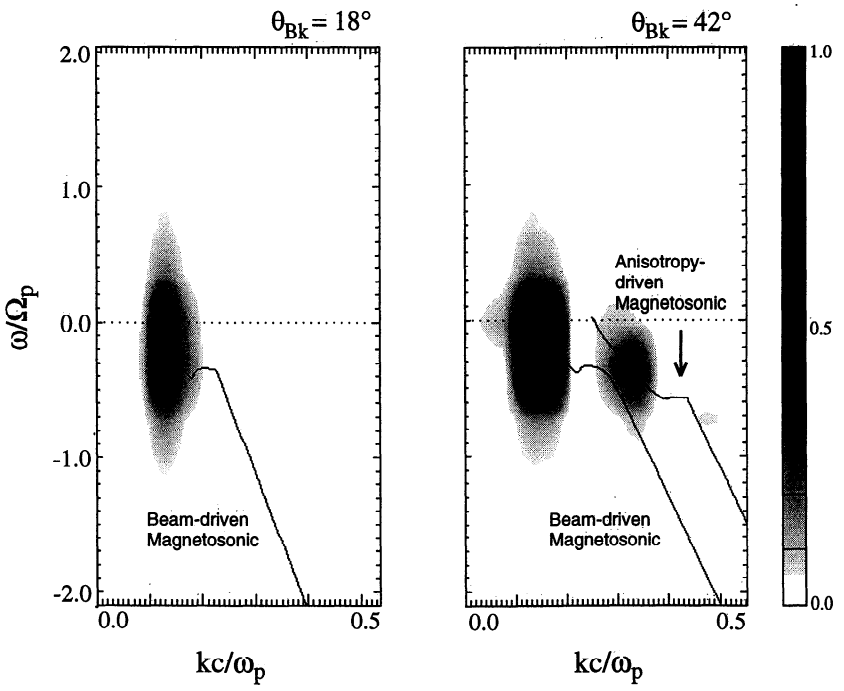

Figure 17. Power spectrum, of B_z for two wave normal angles with the dispersion relations for the beam-driven and anisotropy-driven magnetosonic modes.

agating waves in the simulation, causing interference patterns. In the foreshock, only obliquely propagating waves are present. This issue may be resolved by future driven simulations appropriate for the foreshock.

Two types of simulation have been used in this study; initial value and driven. In the case of the oxygen beam, the two simulations show that very different mechanisms are responsible for the growth of the waves. In the initial value simulation, noncompressional, nonresonant waves are excited first, followed by parallel and obliquely propagating magnetosonic waves which do not steepen. In the driven simulation, oblique magnetosonic waves are dominant from the beginning and steepening is observed. These results indicate that the two types of simulations can have very different outcomes, with the driven simulation being more appropriate for comparison with the observations. This knowledge can be applied to the proton case which we have also studied. Although some steepening has been observed in the results of the initial value proton ring-beam simulation, driven simulations are necessary to properly address the formation of shocklets in the foreshock.

4. Summary and Discussion

In this paper, the linear and nonlinear properties of waves excited by a ring-beam distribution function were investigated. The motivation for this study was to address the excitation and steepening of obliquely propagating magnetosonic waves observed upstream of planetary bow shocks and at comets GZ and GS. We have examined the possibility of the formation of shocklets by means of a ring-beam distribution, which can model both cometary ions and the gyrating ions in the foreshock. We have found that ring-beam distribution functions (which have stability characteristics similar to a beam with a temperature anisotropy) can in general excite waves along the nonresonant, magnetosonic, and Alfvén modes. We have studied two cases, in one the beam ions are oxygen and in the other they are protons. In both cases, two separate instabilities are operative along the magnetosonic branch; one is the beam-driven, which grows due to the beam portion of the distribution and has maximum growth along the magnetic field. The properties of this instability are similar to the right-hand resonant ion/ion instability. The other is the anisotropy-driven magnetosonic mode, which is excited by the ring portion of the distribution function through cyclotron resonance at higher harmonics. As a result, this instability has maximum growth at oblique angles. When the beam density is large, the nonresonant instability has the largest growth, followed by the Alfvén mode, and then finally the two magnetosonic instabilities, which have comparable growth rates. However, at lower beam densities, the Alfvén mode is damped and the nonresonant mode has insignificant growth compared to the magnetosonic instabilities. It has been found that the relationships between the growth rates of the different modes is highly dependent upon the beam density [see *Karimabadi et al.*, 1994].

A study of how these four instabilities compete in the nonlinear regime has been performed using 2-D hybrid simulations. In the case of a field-aligned oxygen beam, first parallel and then later oblique waves are excited. We have shown that these waves are predominantly on the nonresonant mode and do not steepen. Similarly, we have shown that in an initial value oxygen ring-beam simulation parallel propagating nonresonant waves are excited first. When the nonresonant instability saturates, parallel and oblique magnetosonic waves are excited through both the beam-driven and the anisotropy-driven instabilities with maximum power in the oblique direction. In a similar but driven simulation most of the power goes into the obliquely propagating magnetosonic mode, and the waves are shown to steepen and form shocklets. The nonlinear evolution of proton instabilities was investigated using only initial value 2-D hybrid simulations. A proper driven simulation for the foreshock requires nonperiodic boundary condition and will be performed in the future. The initial value simulation of a field-aligned proton beam shows magnetosonic waves growing over a large range of wave normal angles. In agreement with the prediction of linear theory, the maximum power occurs along the magnetic field. Analysis of the wave forms in this simulation shows no sign of wave steepening. The results of the simulation with a proton ring-beam show two peaks in power as a function of propagation angle. One occurs at parallel propagation and the other at oblique angles. The waveforms obtained from this run show evidence of wave steepening; however, the coherence length in the transverse direction is about half of a wavelength, which is somewhat smaller than that observed in the foreshock. This discrepancy may be due to the interference with the parallel propagating waves which are present in the simulations but absent in the foreshock.

The results obtained in this study suggest a number of conclusions. First, it is unlikely that the obliquely propagating compressional magnetosonic waves (shocklets) observed in the foreshock are formed as the result of interaction between the solar wind and the field-aligned beams observed near the ion foreshock boundary. If so, then the monochromatic, sinusoidal magnetosonic waves, which are observed in association with the gyrophase-bunched and intermediate ion distributions are also not related to the shocklets. Evidence for such a conclusion is also present in the observations. For example, as has been discussed by *Le* [1991] and *Le and Russell* [1992], a large number of shocklets have been observed upstream of the bow shock during periods of radial IMF. Since during this geometry the ion foreshock boundary is on the flanks of the shock, it is unlikely that these shocklets were generated by the field-aligned beams coming from the quasi-perpendicular parts of the bow shock. Instead, these observations suggest that the shocklets are formed by ions coming from the quasi-parallel shock. Another piece of evidence comes from the composition measurements of the various ion beam populations in the foreshock [e.g., *Ipavich et al.*, 1988; *Fuselier*, 1994] (S.A. Fuselier et al., Suprathermal He^{2+} in the Earth's foreshock region, submitted to *J. Geo-*

phys. Res., 1995), which show little or no He^{2+} in the field-aligned beams and solar wind type concentrations in the diffuse ion population. These observations suggest that the diffuse ion population does not come about as a result of energy and pitch angle scattering of the field-aligned beams. Since the shocklets are always found to be associated with the diffuse ions, it makes it less likely that they are in any way connected to the field-aligned beams.

Assuming that the shocklets are indeed generated by ion beams originating from the quasi-parallel bow shock, the question of which population is responsible still remains. Using the 1-D hybrid code, *Scholer* [1993] and *Dubouloz and Scholer* [1993] have shown that ion beams with properties similar to the diffuse ion population can excite oblique magnetosonic waves which steepen to form shocklets similar to those observed in the foreshock. However, the problem with diffuse ions is that the maximum growth occurs at parallel propagation, and therefore, one would expect the parallel propagating waves to dominate in a 2-D simulation. On the basis of the results obtained here, we believe a more likely candidate responsible for the excitation of the shocklets is the gyrating ions, which have a ring-beam distribution function and are formed as a result of specular reflection from the quasi-parallel shock. Future driven simulations are needed to further investigate this possibility.

In regards to the formation of shocklets at comets, the results obtained here seem more definitive. This is because the driven simulation model used in the study is much more appropriate for comets. These results suggest that in a cometary environment, the interaction between the solar wind and the cometary ions can lead to the excitation of oblique magnetosonic waves which steepen to form shocklets (under an appropriate production rate). One question that may be raised is why only the oblique waves dominate in such a case. The answer to this question remains unclear; however, it is most likely tied to the time dependent nature of the source, which at the very least would require a source term in the Vlasov equation. It is however possible that even nonlinear effects (such as the scattering of the beam) are also partially responsible for the deviations of the simulation results from the predictions of linear theory.

Acknowledgments. The authors thank Paul Muret for developing the software package that was used for analyzing the wave spectrum and Nicole Mayes for her help with the figures. This research was supported by NASA grants NAGW-1806 and NAG 5-1492. N. Omidi's research was performed under the auspices of the California Space Institute. Computations for this work were performed on the Cray Y-MP and C-90 at the San Diego Supercomputer Center.

The Editor thanks C. W. Smith and D. Papadopoulos for their assistance in evaluating this paper.

References

Akimoto, K., D. Winske, T. B. Onsager, M. F. Thomsen, and S. P. Gary, Steepening of parallel propagating waves into magnetic pulsations: A simulation study, *J. Geophys. Res.*, *96*, 17,599, 1991.

Asbridge, J. R., S. J. Bame, and I. B. Strong, Outward flow of protons from the Earth's bow shock, *J. Geophys. Res.*, *73*, 5777, 1968.

Bame, S. J., J. R. Asbridge, W. C. Feldman, J. T. Gosling, G. Paschmann, and N. Sckopke, Deceleration of the solar wind upstream from the Earth's bow shock and the origin of diffuse upstream ions, *J. Geophys. Res.*, *85*, 2981, 1980.

Bonifazi, C., and G. Moreno, Reflected and diffuse ions backstreaming from the Earth's bow shock, 1, Basic properties, *J. Geophys. Res.*, *86*, 4397, 1981.

Brinca, A., and B. T. Tsurutani, Oblique behavior of low-frequency electromagnetic waves excited by newborn cometary ions, *J. Geophys. Res.*, *94*, 3, 1989.

Dubouloz, N., and M. Scholer, On the origin of short large-amplitude magnetic structures upstream of quasi-parallel collisionless shocks, *Geophys. Res. Lett.*, *20*, 547, 1993.

Eastman, T.E., R.R. Anderson, L.A. Frank, and G.K. Parks, Upstream particles observed in the Earth's foreshock region, *J. Geophys. Res.*, *86*, 4379, 1981.

Fairfield, D. H., Bow shock associated waves observed in the far upstream interplanetary medium, *J. Geophys. Res.*, *74*, 3541, 1969.

Fuselier, S. A., Suprathermal ions upstream and downstream from the Earth's bow shock, in *Solar Wind Sources of Magnetospheric Ultra-Low-Frequency Waves*, *Geophys. Monogr. Ser.*, vol. 81, edited by M. J. Englbretson, K. Takahashi, and M. Scholer, p. 107, AGU, Washington, D. C., 1994.

Fuselier, S. A., M. F. Thomsen, J. T. Gosling, S. J. Bame, and C. T. Russell, Gyrating and intermediate ion distributions upstream from the Earth's bow shock, *J. Geophys. Res.*, *91*, 91, 1986.

Gary, S. P., and C. D. Madland, Electromagnetic ion instabilities in a cometary environment, *J. Geophys. Res.*, *93*, 235, 1988.

Gary, S. P., J. T. Gosling, and D. W. Forslund, The electromagnetic ion beam instability upstream of the Earth's bow shock, *J. Geophys. Res.*, *86*, 6691, 1981.

Gary, S.P., C.W. Smith, M.A. Lee, M.L. Goldstein, and D. W. Forslund, Electromagnetic ion beam instabilities, *Phys. Fluids*, *A*, *27*, 1852, 1984.

Glassmeier, K.-H., and F. M. Neubauer, Low-frequency electromagnetic plasma waves at comet P/Grigg-Skjellerup: Overview and spectral characteristics, *J. Geophys. Res.*, *98*, 20,921, 1993.

Goldstein, M. L., H. K. Wong, and K. H. Glassmeier, Generation of low-frequency waves at comet Halley, *J. Geophys. Res.*, *95*, 947, 1990.

Gosling, J. T., F. R. Asbridge, S. J. Bame, G. Paschmann, and N. Sckopke, Observations of two distinct populations of bow shock ions, *Geophys. Res. Lett.*, *5*, 957, 1978.

Gosling, J. T., M. F. Thomsen, S J. Bame, W. C. Feldman, G. Paschmann, and N. Sckopke, Evidence for specularly reflected ions upstream from the quasi-parallel bow shock, *Geophys. Res. Lett.*, *9*, 1333, 1982.

Gosling, F. T., F. R. Asbridge, S. J. Bame, M. F. Thomsen, and R. D. Zwickl, Large amplitude, low frequency plasma fluctuations at comet Giacobini-Zinner, *Geophys. Res. Lett.*, *13*, 267, 1986.

Greenstadt, E. W., I. M. Green, G. T. Inouye, A. J. Hundhausen, S. J. Bame, and I. B. Strong, Correlated magnetic field and plasma observations of the Earth's bow shock, *J. Geophys. Res.*, *73*, 51, 1968.

Greenstadt, E. W., C. T. Russell, and M. Hoppe, Magnetic field orientation and suprathermal ion streams in the Earth's foreshock, *J. Geophys. Res.*, *85*, 3473, 1980.

Gurgiolo, C., G. K. Parks, B. H. Mauk, C. S. Ling, K. A. Anderson, R. P. Lin, and H. Reme, Non-ExB ordered ion

beams upstream of the Earth's bow shock, *J. Geophys. Res.*, *86*, 4415, 1981.

Hada, T., C. F. Kennel, and T. Terasawa, Excitation of compressional waves and the formation of shocklets in the Earth's foreshock, *J. Geophys. Res.*, *92*, 4423, 1987.

Hoppe, M., and C. T. Russell, Plasma rest frame frequencies and polarizations of the low-frequency upstream waves, ISEE 1 and 2 observations, *J. Geophys. Res.*, *88*, 2021, 1983.

Hoppe, M., C. T. Russell, L. A. Frank, T. E. Eastman, and E. W. Greenstadt, Upstream hydromagnetic waves and their association with backstreaming ion populations: ISEE 1 and 2 observation, *J. Geophys. Res.*, *86*, 4471, 1981.

Hoshino, M., and T. Terasawa, Numerical study of the upstream wave excitation mechanism, 1, Nonlinear phase bunching of beam ion, *J. Geophys. Res.*, *90*, 57, 1985.

Ipavich, F. M., G. Gloeckler, D. C. Hamilton, L. M. Kistler, and J. T. Gosling, Protons and alpha particles in field aligned beams upstream of the bow shock, *Geophys. Res. Lett.*, *15*, 1153, 1988.

Karimabadi, H., D. Krauss-Varban, N. Omidi, S. A. Fuselier, and M. Neugebauer, Low frequency instabilities and the resulting velocity distributions of pickup ions at comet Halley, *J. Geophys. Res.*, **99**, 21,541, 1994.

Le, G., Generation of upstream ULF waves in the Earth's foreshock, Ph.D. thesis, Univ. of Calif., Los Angeles, 1991.

Le, G., and C. T. Russell, A study of ULF wave foreshock morphology, II, Spatial variation of ULF waves, *Planet. Space Sci.*, *40*, 1215, 1992.

Lin, R. P., C. I. Meng, and K. A. Anderson, 30 to 100 keV protons upstream from the Earth's bow shock, *J. Geophys. Res.*, *79*, 489, 1974.

Omidi, N., and D. Winske, Steepening of kinetic magnetosonic waves into shocklets: Simulations and consequences for planetary shocks and comets, *J. Geophys. Res.*, *95*, 2281, 1990.

Omidi, N., H. Karimabadi, D. Krauss-Varban, and K. Killen, Generation and nonlinear evolution of oblique magnetosonic waves: Application to foreshock and comets, in *Solar System Plasma Physics: Resolution of Processes in Space and Time*, *Geophys. Monogr. Ser.*, vol. 84, edited bye J. L. Burch, J. H. Waite, pp. 71–84, AGU, Washingtn, D.C., 1994.

Paschmann, G., N. Sckopke, S. J. Bame, J. R. Asbridge, J. T. Gosling, C. T. Russell, and E. W. Greenstadt, Association of low frequency waves with supra-thermal ions in the upstream solar wind, *Geophys. Res. Lett.*, *6*, 209, 1979.

Paschmann, G., N. Sckopke, I. Papamastorakis, J. R. Asbridge, S. J. Bame, and J. T. Gosling, Characteristics of reflected and diffuse ions upstream from the Earth's bow shock, *J. Geophys. Res.*, *86*, 4355, 1981.

Russell, C. T., D. D. Childers, and P. J. Coleman, Jr., OGO5 Observations of upstream waves in interplanetary medium: Discrete wave packets, *J. Geophys. Res.*, *76*, 845, 1971.

Scholer, M., Upstream waves, shocklets, short large-amplitude magnetic structures and the cyclic behavior of oblique quasi-parallel collisionless shocks, *J. Geophys. Res.*, *98*, 47, 1993.

Sckopke, N., G. Paschmann, S. J. Bame, J. T. Gosling, and C. T. Russell, Evolution of ion distributions across the nearly perpendicular bow shock, specularly and nonspecularly reflected ions, *J. Geophys. Res.*, *88*, 6121, 1983.

Smith, E. J., B. T. Tsurutani, J. A. Slavin, D. E. Jones, G. L. Siscoe, and D. A. Mendis, International cometary explorer encounter with Giacobini-Zinner: Magnetic field observations, *Science*, *232*, 382, 1986.

Thomsen, M. F., S. J. Schwartz, and J. T. Gosling, Observational evidence on the origin of ions upstream of the Earth's bow shock, *J. Geophys. Res.*, *88*, 7843, 1983b.

Thomsen, M. F., G. T. Gosling, S. J. Bame, and C. T. Russell, Gyrating ions and large amplitude monochromatic MHD waves upstream of the Earth's bow shock, *J. Geophys. Res.*, *90*, 267, 1985.

Tsurutani, B. T., and E. J. Smith, Strong hydromagnetic turbulence associated with comet Giacobini-Zinner, *Geophys. Res. Lett.*, *13*, 259, 1986a.

Tsurutani, B. T. and E. J. Smith, Hydromagnetic waves and instabilities associated with cometary ion pickup: ICE observations, *Geophys. Res. Lett.*, *13*, 263, 1986b.

Tsurutani, B. T., R. M. Thorne, E. J. Smith, J. T. Gosling, and H. Matsumoto, Steepened magnetosonic waves at comet Giacobini-Zinner, *J. Geophys. Res.*, *92*, 11,074, 1987.

Winske, D., and M. M. Leroy, Diffuse ions produced by electromagnetic ion beam instabilities, *J. Geophys. Res.*, *89*, 2673, 1984.

Winske, D., and S. P. Gary, Electromagnetic instabilities driven by cool heavy ion beams, *J. Geophys. Res.*, *91*, 6825, 1986.

Winske, D., C. S. Wu, Y. Y. Li, D. D. Mou, and S. Y. Guo, Coupling of newborn ions to the solar wind by electromagnetic instabilities and their interaction with the bow shock, *J. Geophys. Res.*, *90*, 2756, 1985.

Wong, H. K., M. L. Goldstein, C. W. Smith, Ion cyclotron harmonic resonances driven by ion ring-beam distributions, *J. Geophys. Res.*, *96*, 285, 1991.

H. Karimabadi, K. Killen, D. Krauss-Varban, and N. Omidi, Department of Electrical and Computer Engineering, University of California, San Diego, La Jolla, CA 92093-0407 (e-mail: killen@ece.ucsd.edu).

(Received September 4, 1994; revised November 2, 1994; accepted November 3, 1994.)